Analyst

ROYAL SOCIETY OF CHEMISTRY

PAPER

View Article Online
View Journal | View Issue

Cite this: *Analyst*, 2022, **147**, 4222

A tracer-type fluorescent probe for imaging adenosine triphosphate under the stresses of hydrogen sulfide and hydrogen peroxide in living cells†

Leilei Yao,[a] Weijie Zhang,[b] Caixia Yin, *[b] Yongbin Zhang[a] and Fangjun Huo *[a]

Adenosine triphosphate (ATP) is a direct energy source in cells and the core of the biochemical system, and is closely related to various metabolic activities in living organisms. Therefore, designing a simple and rapid ATP detection method is significant to study its physiological function. Herein, a dual-channel fluorescent probe ***RhB-NA*** for the *in situ* imaging of ATP in living cells was designed and synthesized. When ATP bound to ***RhB-NA***, the spirolactam in rhodamine B was induced to open, resulting in a new fluorescence response at 589 nm. Notably, in cell imaging, the treatment of HeLa cells with exogenous H_2O_2 and H_2S, which have certain effects on the mitochondria, confirmed that ***RhB-NA*** could detect fluctuations in ATP levels after the mitochondrial state was affected. We believe that ***RhB-NA*** has far-reaching significance for studying certain physiological diseases caused by abnormal ATP levels.

Received 2nd August 2022,
Accepted 15th August 2022

DOI: 10.1039/d2an01262f

rsc.li/analyst

Introduction

Adenosine triphosphate (ATP), as one of the nucleoside polyphosphates (NPPs), is known as the universal energy currency within cells due to it being the most direct source of energy in cells,[1,2] and plays an important role in cellular energy metabolism and signal transduction.[3–6] Meanwhile, in living organisms, ATP participates in a variety of essential biological processes.[7,8] Abnormal levels of ATP have an impact on some physical functions, which can cause the occurrence of many diseases, such as certain malignant tumors/cancers, Parkinson's disease (PD), and cardiovascular disease.[9–12] Hence, in clinical diagnosis, the ATP level can be used as an important monitoring index for many diseases, and developing a detection platform with high specificity is an attractive goal for the early diagnosis of ATP-related diseases.

ATP is traditionally detected by electrophoresis (EP), isotope tracers (ITM), chemiluminescence (CL), *etc.*[13] However, because of the long test time, complex test procedure and inability to well image ATP in living cells, these methods do not meet the current research requirements. Thus, we must find a novel method to monitor ATP in living cells. In recent years, fluorescent probe imaging technology has been further developed in biomolecule detection due to its low cost, fast detection speed, and real-time imaging in living cells.[14–19] However, in recent decades, there have only been a few reports on small-molecule fluorescent probes for ATP detection, mainly through the opening of the spirolactam in rhodamine to release fluorescence for simple identification.[20–24] More importantly, few probes have been reported that can simultaneously recognize ATP and track the probe to improve detection accuracy.[25–27] Therefore, the design of highly selective and sensitive ATP detection probes is still an urgent problem to be solved.

Herein, we report a novel two-channel fluorescent probe ***RhB-NA*** (Scheme 1), in which diethylenetriamine was chosen as a linker and reaction site for ATP, the fluorescence of rhodamine was utilized for ATP imaging, and the fluorescence of naphthalimide was used for probe tracking. ***RhB-NA*** fluoresced naphthalimide when the ring in rhodamine B was closed; with the addition of ATP, the spirolactam structure of rhodamine B is opened, resulting in a new intense optical signal.

Furthermore, given that ATP is mainly produced in the mitochondria, the detection of cellular endogenous ATP levels by ***RhB-NA*** in different mitochondrial states was investigated. In previous reports, changes in the levels of H_2S[28,29] and H_2O_2[30,31] in cells were found to have certain effects on the mitochondrial state. Thus, the relationships between intra-

[a]*Research Institute of Applied Chemistry, Shanxi University, Taiyuan 030006, China. E-mail: huoff@sxu.edu.cn*
[b]*Institute of Molecular Science, Key Laboratory of Chemical Biology and Molecular Engineering of Ministry of Education, Shanxi University, Taiyuan 030006, China. E-mail: yincx@sxu.edu.cn*

† Electronic supplementary information (ESI) available. See DOI: https://doi.org/10.1039/d2an01262f

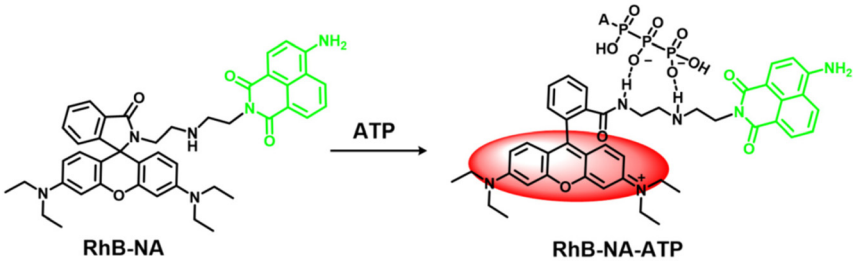

Scheme 1 Response mechanism of ***RhB-NA*** for ATP.

cellular ATP and exogenous H_2S and H_2O_2 were analyzed. Cell imaging was performed with two fluorescence channels: the green channel (λ_{ex} = 458 nm, λ_{em} = 510–550 nm) and the red channel (λ_{ex} = 561 nm, λ_{em} = 580–620 nm). We observed that the fluorescence intensity of the red channel increased after H_2S stimulation, while that of the green channel had no obvious change; after stimulation with H_2O_2, the fluorescence intensity of the red channel weakened, and that of the green channel again had no significant change. As the result, a method was developed that can trace the probe and detect changes in ATP levels caused by H_2S and H_2O_2.

Experiments

Materials

Relevant instruments and materials can be found in the ESI.†

Synthesis of *RhB-NA*

The probe ***RhB-NA*** was synthesized according to the route shown in Scheme 1 *via* 3 steps. Compound 2[32] and compound 5[33] were synthesized according to the procedure reported in a previous work. Then, compound 2 (213 mg, 1 mmol) and compound 5 (528 mg, 1 mmol) were dissolved in ethanol (15 mL), and the mixture was refluxed for 10 h at 80 °C. Later, the solvent was distilled under reduced pressure, and the crude product was purified with silica gel column chromatography (CH_3OH/CH_2Cl_2, 1 : 20, v/v), affording the probe as a yellow solid (540 mg, yield 74%). The ^1H NMR and ^{13}C NMR spectra and HR-MS results of the probe are shown in Fig. S1–S3.† ^1H NMR (600 MHz, DMSO) δ 8.60 (d, J = 8.3 Hz, 1H), 8.37 (d, J = 7.3 Hz, 1H), 8.14 (d, J = 8.4 Hz, 1H), 7.76 (m, 1H), 7.63 (s, 1H), 7.53 (m, 2H), 7.42 (s, 2H), 7.00 (d, J = 8.3 Hz, 1H), 6.82 (d, J = 8.4 Hz, 1H), 6.32 (d, J = 19.9, 9.0 Hz, 6H), 3.92 (s, 2H), 3.27 (q, J = 7.1 Hz, 8H), 3.05 (d, J = 7.1 Hz, 2H), 2.70 (s, 2H), 2.23 (s, 2H), 1.03 (t, J = 7.0 Hz, 12H). ^{13}C NMR (151 MHz, DMSO) δ 167.53, 164.27, 163.38, 153.78, 153.11, 153.10, 148.86, 134.31, 133.03, 131.37, 131.00, 130.17, 129.70, 128.71, 128.66, 124.37, 124.03, 122.71, 122.31, 119.84, 108.64, 108.59, 108.10, 105.55, 97.75, 64.47, 47.20, 47.04, 46.17, 44.10, 40.59, 40.47, 40.33, 40.19, 40.05, 39.91, 39.77, 39.63, 39.09, 33.74, 15.21, 12.80. HR-MS: m/z calcd for the probe ($C_{44}H_{46}N_6O_4$, $[M + H]^+$), 723.3581; found, 723.3646 (Scheme 2).

Photochemical properties of *RhB-NA* measurement

A stock solution of ***RhB-NA*** required for property testing was made by dissolving the probe in DMSO. ATP stock solution, other ionic stock solutions and other biomolecule stock solutions were prepared by dissolving their solids in PBS buffer solution.

Living cell culture and imaging

HeLa cells were cultured in Dulbecco's modified Eagle's medium containing 10% fetal bovine serum and grown in an incubator at 37 °C for approximately 24 h. Fluorescence signals were collected for the red channel: 580–620 nm (λ_{ex} = 561 nm) and green channel: 510–550 nm (λ_{ex} = 458 nm).

Results and discussion

Design of the probe *RhB-NA* and its sensing mechanism for ATP

The probe ***RhB-NA*** was designed based on the high fluorescence quantum yield and the spirolactam structure of rhodamine B, to which diethylenetriamine was attached as the reactive site for ATP. For the purpose of probe tracking, the naphthalimide fluorophore was chosen as the "tracer" after ***RhB-NA*** entered the cells, so that ***RhB-NA*** can be displayed in the cells before and after the reaction with ATP.

We found that the fluorescence recognition of ***RhB-NA*** towards ATP was carried out through the ring-opening of the spirolactam in rhodamine B. As shown in Scheme 1, when the ring of rhodamine B was closed, ***RhB-NA*** was stable and only showed fluorescence from naphthalimide.

The two NH protons contained in ***RhB-NA*** can combine with the triphosphate group of ATP through hydrogen bonds. Further, the intermolecular interactions can be strengthened through the π–π bonds between the base of ATP and the rhodamine of ***RhB-NA***. Ultimately, significant fluorescence emission occurred due to the opening of the spirolactam ring. This reaction mechanism has been reported previously.[8]

Spectral characteristics of *RhB-NA*

The recognition of the probe ***RhB-NA*** towards ATP was studied by utilizing absorption and fluorescence spectroscopy in PBS buffer. First, the UV-Vis spectra (Fig. 1a) of ***RhB-NA*** were recorded in PBS buffer. It can be seen that the pure probe

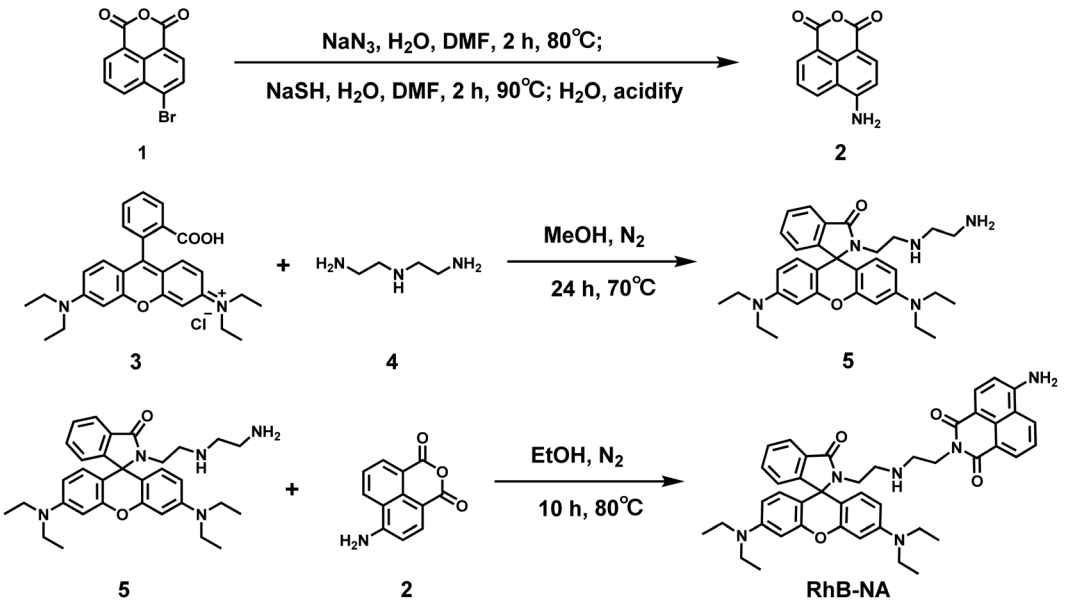

Scheme 2 Synthesis of ***RhB-NA***.

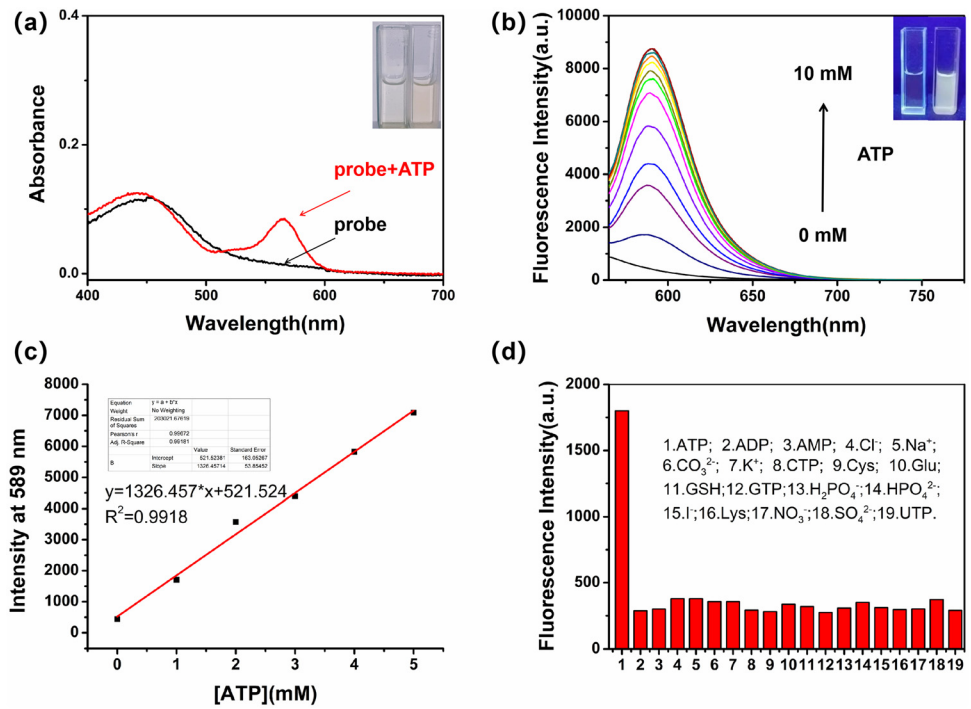

Fig. 1 (a) Absorption spectrum changes of ***RhB-NA*** (10 μM) upon the addition of ATP (10 mM). Inset: a photograph of ***RhB-NA*** before and after the addition of ATP (10 mM) under natural light. (b) Fluorescence spectra of ***RhB-NA*** (10 μM, λ_{ex} = 550 nm). Inset: a photograph of ***RhB-NA*** before and after the addition of 10 mM ATP under a handheld UV light. (c) Linear relationship of the fluorescence intensity of ***RhB-NA*** with different ATP levels (0–5 mM). (d) Fluorescence intensity at 589 nm of ***RhB-NA*** (10 μM) upon the addition of other species (1 mM) (1. ATP; 2. ADP; 3. AMP; 4. Cl^-; 5. Na^+; 6. CO_3^{2-}; 7. K^+; 8. CTP; 9. Cys; 10. Glu; 11. GSH; 12. GTP; 13. $H_2PO_4^-$; 14. HPO_4^{2-}; 15. I^-; 16. Lys; 17. NO_3^-; 18. SO_4^{2-}; 19. UTP) (λ_{em} = 562 nm, λ_{ex} = 550 nm, slit: 5 nm/5 nm). The reactions were performed in PBS buffer solution.

exhibited an obvious absorption peak at 451 nm; after adding ATP (10 mM), a distinct absorption peak appeared at 566 nm. A color change of the solution occurred from pale yellow to pale pink. The result indicates that ATP induced the opening of the spirolactam ring on the rhodamine B fluorophore and the absorption peak of naphthalimide did not disappear. Therefore, we believe that this process is without fluorescence resonance energy transfer (FRET).

Subsequently, we performed the ATP fluorescence titration experiment of ***RhB-NA*** in the same system. Fig. 1b shows the fluorescence changes of ***RhB-NA*** in response to different levels of ATP. The figure shows the negligible intensity at 589 nm when the free probe was excited at 550 nm; upon the addition of ATP, a significant increase in fluorescence at 589 nm was observed, followed by the saturation of fluorescence intensity (an almost 20-fold increase in fluorescence) with the addition of 10 mM ATP.

In addition, a good linear relationship between the fluorescence intensity and the ATP levels (0–5 mM) is displayed in Fig. 1c (R^2 = 0.9918, k = 1326.457). The detection limit is 0.002 mM, which demonstrated that the probe can detect ATP efficiently and sensitively.

Selectivity studies

Selectivity is a significant parameter to determine the performance of a novel fluorescent probe. To verify the specificity of ***RhB-NA*** for ATP detection, certain species were chosen for selective experiments. Various common interfering ions such as Cl^-, Na^+, CO_3^{2-}, K^+, $H_2PO_4^-$, HPO_4^{2-}, I^-, NO_3^-, SO_4^{2-}; energy-relevant molecules such as ADP, AMP, CTP, GTP, and UTP; and amino acids such as Cys, Glu, GSH, and Lys were chosen. They were separately added to a system of PBS (pH = 7.4) containing ***RhB-NA*** (10 μM). As shown in Fig. 1d, no obvious fluorescence responses appeared, which clearly confirmed that the designed probe ***RhB-NA*** exhibited high selectivity towards ATP. This result may be due to the presence of hydrogen bonding forces between the phosphate moiety of ATP and the diethylenetriamine of ***RhB-NA***.

Cellular imaging

We found that ***RhB-NA*** responded well to ATP in *in vitro* experiments. To further explore the cell permeability of ***RhB-NA***, living-cell confocal fluorescence imaging experiments were performed. Before conducting the cell imaging experiments, the cytotoxicity of ***RhB-NA*** towards HeLa cells was explored using CCK-8 assays (Fig. S4†). The results show that ***RhB-NA*** has low cytotoxicity, proving the potential of this probe for biological applications.

Excitation wavelengths of 561 nm and 458 nm were used to evaluate the ability of ***RhB-NA*** to image ATP in living cells. Co-incubating ***RhB-NA*** with HeLa cells for 10 min, we found that the red channel (λ_{ex} = 561 nm, λ_{em} = 580–620 nm) and green channel (λ_{ex} = 458 nm, λ_{em} = 510–550 nm) both showed obvious fluorescence, indicating that ***RhB-NA*** has good membrane permeability and can sensitively detect intracellular ATP (Fig. S5†). Moreover, within 15 min of ***RhB-NA*** completely entering the cells, the red channel showed a trend of fluorescence enhancement over time, while the green channel showed no obvious fluorescence change (Fig. 2), indicating that ***RhB-NA*** can sensitively monitor the dynamic variation of intracellular ATP.

In addition, to the best of our knowledge, H_2S is able to act as a mitochondrial energy donor to stimulate ATP production, and H_2O_2 can cause mitochondrial damage, thereby affecting ATP levels. Subsequently, the effects of exogenous H_2S and H_2O_2 on ATP in living cells were analyzed. HeLa cells were treated with Na_2S solution (10 μM) for 10 min before adding ***RhB-NA*** (10 μM) and then incubated for 10 min. As shown in Fig. 3, fluorescence enhancement was found using confocal microscopy, indicating that increased intracellular H_2S levels stimulated increased ATP levels. We believe that ***RhB-NA*** can detect the fluctuations in ATP levels caused by H_2S.

Next, exogenous H_2O_2 (500 μM) was preincubated with HeLa cells for 10 min, and ***RhB-NA*** (10 μM) was then added and incubated for 10 min. Confocal imaging (Fig. 4) showed that the fluorescence intensity of the green channel did not change significantly, while the red channel showed almost no fluorescence. In order to further demonstrate that ***RhB-NA*** can

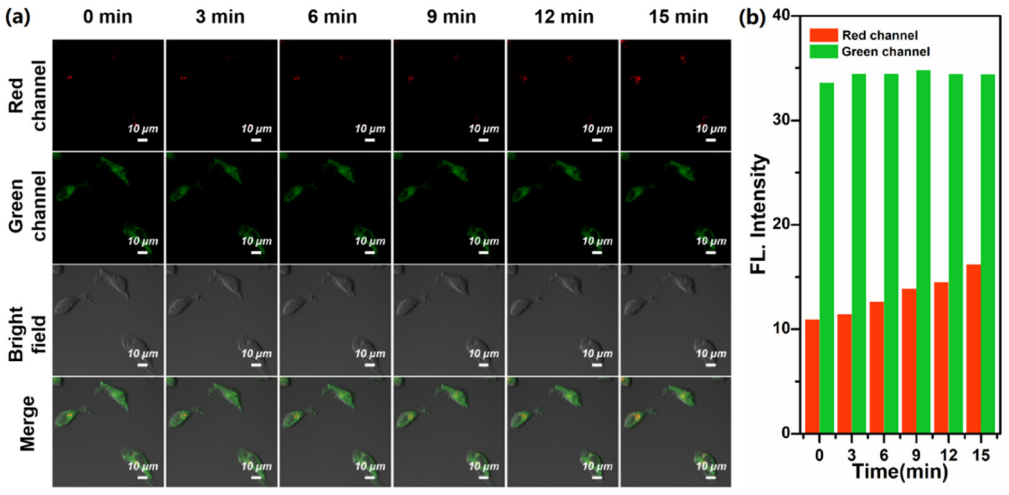

Fig. 2 (a) Confocal microscopy fluorescence images of HeLa cells induced by ***RhB-NA*** (10 μM) for 0–15 min and (b) the corresponding mean fluorescence intensities of the red and green channels. Red channel: λ_{ex} = 561 nm, λ_{em} = 580–620 nm; green channel: λ_{ex} = 458 nm, λ_{em} = 510–550 nm. Scale bar: 10 μm.

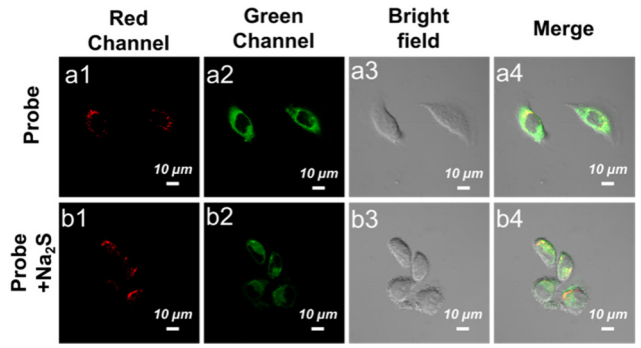

Fig. 3 Confocal microscopy fluorescence images for ATP in living HeLa cells. HeLa cells were incubated with (a) ***RhB-NA*** (10 μM) for 10 min; (b) Na_2S (10 μM) for 10 min and then ***RhB-NA*** (10 μM) for 10 min. Red channel: λ_{ex} = 561 nm, λ_{em} = 580–620 nm; green channel: λ_{ex} = 458 nm, λ_{em} = 510–550 nm. Scale bar: 10 μm.

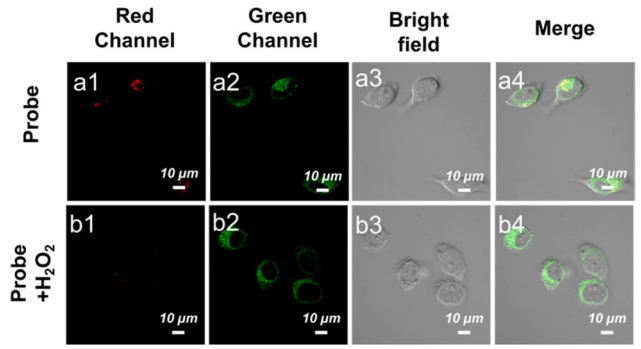

Fig. 4 Confocal microscopy fluorescence images for ATP in living HeLa cells. HeLa cells were incubated with (a) ***RhB-NA*** (10 μM) for 10 min; (b) H_2O_2 (500 μM) for 10 min, then ***RhB-NA*** (10 μM) for 10 min. Red channel: λ_{ex} = 561 nm, λ_{em} = 580–620 nm; green channel: λ_{ex} = 458 nm, λ_{em} = 510–550 nm. Scale bar: 10 μm.

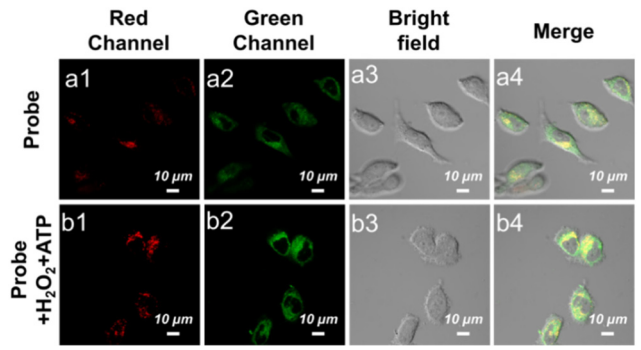

Fig. 5 Confocal microscopy fluorescence images of ***RhB-NA*** for ATP in living HeLa cells. HeLa cells were incubated with (a) ***RhB-NA*** (10 μM) for 10 min; (b) H_2O_2 (500 μM) for 10 min, probe (10 μM) for 10 min and then exogenous ATP (1 mM) for 10 min. Red channel: λ_{ex} = 561 nm, λ_{em} = 580–620 nm; green channel: λ_{ex} = 458 nm, λ_{em} = 510–550 nm. Scale bar: 10 μm.

detect the H_2O_2-induced decrease in ATP levels, HeLa cells were treated with H_2O_2 (500 μM) for 10 min, followed by ***RhB-NA*** (10 μM) for 10 min, and finally exogenous ATP (1 mM) for 10 min. Confocal imaging (Fig. 5) showed that the fluorescence intensity of the green channel did not change significantly. The red channel fluoresced strongly. Therefore, we can conclude that ***RhB-NA*** can detect the decrease in ATP levels due to a large amount of H_2O_2 stimulation. We attribute this phenomenon to H_2O_2 causing damage to mitochondrial function, thereby limiting ATP levels.

Conclusion

In summary, a novel dual-channel fluorescent probe was developed, which provides a specific fluorescence response to ATP *in vivo* and *in vitro*, with high sensitivity, good biocompatibility, and membrane permeability. Moreover, ***RhB-NA*** was successfully applied to image endogenous and exogenous ATP in living cells. Importantly, ***RhB-NA*** can be used to sensitively detect intracellular ATP level changes caused by H_2S and H_2O_2. More interestingly, the fluorescence of naphthalimide in ***RhB-NA*** can be applied to track its entry into cells in real-time, which has potential value for further clinical application-related research.

Conflicts of interest

There are no conflicts to declare.

Acknowledgements

We thank the National Natural Science Foundation of China (No. 22074084), One Hundred People Plan of Shanxi Province, Shanxi Province "1331 project" Key Innovation Team Construction Plan Cultivation Team (2018-CT-1), 2018 Xiangyuan County Solid Waste Comprehensive Utilization Science and Technology Project (2018XYSDJS-05), Shanxi Province Foundation for Returnees (2017-026), Shanxi Collaborative Innovation Center of High Value-added Utilization of Coal-related Wastes (2015-10-B3), the Shanxi Province Foundation for Selected (No. 2019), Innovative Talents of Higher Education Institutions of Shanxi, Scientific and Technological Innovation Programs of Higher Education Institutions in Shanxi (2019L0031), Key R&D Program of Shanxi Province (201903D421069), the Shanxi Province Science Foundation (No. 20210302124012, 201901D111015), and the Shanxi University Graduate Innovation Project and Scientific Instrument Center of Shanxi University (201512).

References

1 Y. Zhou, Z. Xu and J. Yoon, *Chem. Soc. Rev.*, 2011, **40**, 2222–2235.

2 H. Singh, S. Sreedharan, R. Tiwari, C. Walther, C. Smythe, S. K. Pramanik, J. A. Thomas and A. Das, *Cryst. Growth Des.*, 2018, **18**, 7199–7206.
3 D. A. Cockayne, S. G. Hamilton, Q.-M. Zhu, P. M. Dunn, Y. Zhong, S. Novakovic, A. B. Malmberg, G. Cain, A. Berson, L. Kassotakis, L. Hedley, W. G. Lachnit, G. Burnstock, S. B. McMahon and A. P. D. W. Ford, *Nature*, 2000, **407**, 1011–1015.
4 P. Yu, X. He, L. Zhang and L. Mao, *Anal. Chem.*, 2015, **87**, 1373–1380.
5 E. H. Abraham, P. Okunieff, S. Scala, P. Vos, M. J. S. Oosterveld, A. Y. Chen, B. Shrivastav and G. Guidotti, *Science*, 1997, **275**, 1324–1326.
6 S. Zhang, Y. Yan and S. Bi, *Anal. Chem.*, 2009, **81**, 8695–8701.
7 Z. Xu, G. Zeng, Y. Liu, X. Zhang, J. Cheng, J. Zhang, Z. Ma, M. Miao, D. Zhang and Y. Wei, *Dyes Pigm.*, 2019, **163**, 559–563.
8 Z. Li, S. Li, Y. Guo, C. Yuan, X. Yan and K. S. Schanze, *ACS Nano*, 2021, **15**, 4979–4988.
9 T. B. Ren, S. Y. Wen, L. Wang, P. Lu, B. Xiong, L. Yuan and X. B. Zhang, *Anal. Chem.*, 2020, **92**, 4681–4688.
10 B. Huang, B. Liang, R. Zhang and D. Xing, *Coord. Chem. Rev.*, 2022, **452**, 214302.
11 T. Lee, P. Seeman, A. Rajput, I. J. Farley and O. Hornykiewicz, *Nature*, 1978, **273**, 59–61.
12 Y. Liu, Y.-H. Geng, H. Yang, H. Yang, Y.-T. Zhou, H.-Q. Zhang, X.-X. Tian and W.-G. Fang, *Cancer Lett.*, 2018, **430**, 1–10.
13 X. Zheng, R. Peng, X. Jiang, Y. Wang, S. Xu, G. Ke, T. Fu, Q. Liu, S. Huan and X. Zhang, *Anal. Chem.*, 2017, **89**, 10941–10947.
14 A. Paganin-Gioanni, E. Bellard, L. Paquereau, V. Ecochard, M. Golzio and J. Teissié, *Radiol. Oncol.*, 2010, **44**, 142–148.
15 J. Rao, A. Dragulescu-Andrasi and H. Yao, *Curr. Opin. Biotechnol*, 2007, **18**, 17–25.
16 A. K. Singh, A. V. Nair and N. D. P. Singh, *Anal. Chem.*, 2022, **94**, 177–192.
17 D. Wu, A. C. Sedgwick, T. Gunnlaugsson, E. U. Akkaya, J. Yoon and T. D. James, *Chem. Soc. Rev.*, 2017, **46**, 7105–7123.
18 Y. Zhang, G. Qi, B. Wang, D. Wang and Y. Jin, *Anal. Chem.*, 2020, **92**, 3882–3887.
19 Z. Liu, W. He and Z. Guo, *Chem. Soc. Rev.*, 2013, **42**, 1568–1600.
20 W. Lang, G. Cheng, R. Peng and Q.-Y. Cao, *Dyes Pigm.*, 2021, **189**, 109245.
21 T. Kowada, H. Maeda and K. Kikuchi, *Chem. Soc. Rev.*, 2015, **44**, 4953–4972.
22 Y. Zhou, F. Wang, Y. Kim, S.-J. Kim and J. Yoon, *Org. Lett.*, 2009, **11**, 4442–4445.
23 R. Zhang, F. Yan, Y. Huang, D. Kong, Q. Ye, J. Xu and L. Chen, *RSC Adv.*, 2016, **6**, 50732–50760.
24 W. Zhang, Y. Lv, F. Huo, Y. Zhang and C. Yin, *Dyes Pigm.*, 2022, **204**, 110442.
25 X. Jin, X. Wu, B. Wang, P. Xie, Y. He, H. Zhou, B. Yan, J. Yang, W. Chen and X. Zhang, *Sens. Actuators, B*, 2018, **261**, 127–134.
26 Z. Xu, G. Zeng, Y. Liu, X. Zhang, J. Cheng, J. Zhang, Z. Ma, M. Miao, D. Zhang and Y. Wei, *Dyes Pigm.*, 2019, **163**, 559–563.
27 K. M. K. Swamy, S. Eom, Y. Liu, G. Kim, D. Lee and J. Yoon, *Sens. Actuators, B*, 2019, **281**, 350–358.
28 C. Szabo and M. R. Hellmich, *Cell Cycle*, 2013, **12**, 2915–2916.
29 B. D. Paul, S. H. Snyder and K. Kashfi, *Redox Biol.*, 2021, **38**, 101772.
30 Z. Wu, M. Liu, Z. Liu and Y. Tian, *J. Am. Chem. Soc.*, 2020, **142**, 7532–7541.
31 J. Williamson and G. Davison, *Antioxidants*, 2020, **9**, 1142.
32 B. Bag and B. Biswal, *Org. Biomol. Chem.*, 2012, **10**, 2733–2738.
33 Y. Fang, W. Shi, Y. Hu, X. Li and H. Ma, *Chem. Commun.*, 2018, **54**, 5454–5457.